J Neuropathol Exp Neurol
Vol. 73, No. 5
May 2014
pp. 442–453


ORIGINAL ARTICLE

OPEN

# JC Virus Inclusions in Progressive Multifocal Leukoencephalopathy: Scaffolding Promyelocytic Leukemia Nuclear Bodies Grow With Cell Cycle Transition Through an S-to-G2–Like State in Enlarging Oligodendrocyte Nuclei

Yukiko Shishido-Hara, MD, PhD, Takuya Yazawa, MD, PhD, Motoo Nagane, MD, PhD, Kayoko Higuchi, MD, PhD, Shiho Abe-Suzuki, MD, PhD, Morito Kurata, MD, PhD, Masanobu Kitagawa, MD, PhD, Hiroshi Kamma, MD, PhD, and Toshiki Uchihara, MD, PhD

**Abstract**

In progressive multifocal leukoencephalopathy, JC virus–infected oligodendroglia display 2 distinct patterns of intranuclear viral inclusions: full inclusions in which progeny virions are present throughout enlarged nuclei and dot-shaped inclusions in which virions are clustered in subnuclear domains termed ''promyelocytic leukemia nuclear bodies'' (PML-NBs). Promyelocytic leukemia nuclear bodies may serve a scaffolding role in viral progeny production. We analyzed the formation process of intranuclear viral inclusions by morphometry and assessed PML-NB alterations in the brains of 2 patients with progressive multifocal leukoencephalopathy. By immunohistochemistry, proliferating cell nuclear antigen was most frequently detected in smaller nuclei; cyclin A was detected in larger nuclei. This suggests an S-to-G2 cell cycle transition in infected cells associated with nuclear enlargement. Sizes of PML-NBs were variable, but they were usually either small speckles 200 to 400 nm in diameter or distinct spherical shells with a diameter of 1 μm or more. By confocal microscopy, JC virus capsid proteins were associated with both small and large PML-NBs, but disruption of large PML-NBs was observed by ground-state depletion fluorescence nanoscopy. Clusters of progeny virions were also detected by electron microscopy. Our data suggest that, in progressive multifocal leukoencephalopathy, JC virus produces progeny virions in enlarging oligodendrocyte nuclei in association with growing PML-NBs and with cell cycle transition through an S-to-G2-like state.

**Key Words**: Cell cycle, Cell stress, Intranuclear viral inclusions, JC virus, PML-NBs, Progressive multifocal leukoencephalopathy.

## INTRODUCTION

Progressive multifocal leukoencephalopathy is a fatal demyelinating disorder caused by opportunistic infection with a small DNA virus, human polyomavirus JC (also known as and hereafter referred to as JC virus) (1). Central nervous system oligodendrocytes are a major target of JC virus infection, and infected cells harbor progeny virions in markedly enlarged nuclei. In routine hematoxylin and eosin (H&E)–stained sections, intranuclear viral inclusions are characterized as amphiphilic materials dispersed throughout the nucleoplasm (full inclusions). Recently, however, immunohistochemistry has revealed the presence of dot-shaped intranuclear inclusions, which reflect JC virus progeny virions clustered at distinct subnuclear domains called ''promyelocytic leukemia nuclear bodies'' (PML-NBs) (note that ''PML'' herein refers only to promyelocytic leukemia and not to progressive multifocal leukoencephalopathy) (2–4). Production of viral progeny frequently occurs in specific intracellular compartments (5, 6). Promyelocytic leukemia nuclear bodies support JC virus proliferation, likely providing scaffolding for capsid assembly linked to viral genomic DNA replication.

Promyelocytic leukemia nuclear bodies are ubiquitously present in eukaryotic nuclei and regulate a variety of nuclear functions (7–11). Each nucleus usually contains 1 to 30 PML-NBs with diameters of 0.2 to 1 μm, but the numbers and sizes of PML-NBs change dynamically during the cell cycle. In G0 phase, the fewest PML-NBs are observed, and the numbers increase by a fission mechanism in early S phase. Thus, there are approximately twice as many PML-NBs in G2 as in G1 (12). Giant PML-NBs may appear under specific disease conditions, and they are shaped as spherical shells more than 1 μm in diameter in G2 phase (13). Promyelocytic

From the Departments of Pathology (YS-H, TY, HK) and Neurosurgery (MN), Kyorin University School of Medicine, Shinkawa, Mitaka; Laboratory of Structural Neuropathology, Tokyo Metropolitan Institute for Medical Science, Kamikitazawa, Setagaya-ku (YS-H, TU); Department of Comprehensive Pathology, Graduate School of Medical and Dental Sciences, Tokyo Medical and Dental University, Yushima, Bunkyo-ku (SA-S, Mku, MKi), Tokyo; and Section of Pathology, Aizawa Hospital, Honjo, Matsumoto, Nagano (KH), Japan.

Send correspondence and reprint requests to: Yukiko Shishido-Hara, MD, PhD, Department of Pathology, Kyorin University School of Medicine, 6-20-2 Shinkawa, Mitaka, Tokyo 181-8611, Japan; E-mail: yhara@ks.kyorin-u.ac.jp

This work was supported by a Grant-in-Aid for Scientific Research from the Ministry of Education, Culture, Sports, Science, and Technology of Japan (Grant 24590428 to Yukiko Shishido-Hara) and by a grant from the Research Committee of Prion Disease and Slow Virus Infection, the Ministry of Health, Labor, and Welfare of Japan.

The authors have no conflict of interest to declare.

leukemia nuclear bodies partition during mitosis and are re-established in G1 phase (14, 15).

Many DNA viruses, including JC virus, preferentially interact with PML-NBs during viral proliferation (16–19). We previously demonstrated that JC virus major capsid protein VP1 and minor capsid proteins VP2 and VP3 cooperatively transport to the nucleus and accumulate at PML-NBs, where they are assembled into capsids in vitro (20–22). Intranuclear PML-NB targeting is a process that is distinct from nuclear transport, however, because PML-NB accumulation of JC virus capsid proteins was abolished by deleting the putative DNA-binding domain encoded on the common C-terminal sequence of VP2/VP3 (22). (The VP3 sequence is identical to two thirds of the C-terminal VP2 sequence; thus, it is termed ''VP2/VP3.'') The capsid protein DNA-binding domain likely plays a role in PML-NB targeting because the viral DNA replication foci of polyomaviruses are linked to PML-NBs (23). In glial cells of human brain tissues, we previously identified large PML-NBs, which were shaped as spherical shell structures more than 1 μm in diameter with a shell thickness of 300 to 400 nm (4). Thus, it has been suggested that both viral DNA replication and viral capsid formation actively occur at these PML-NBs in the human brains. The large PML-NBs may represent an anti-stress response associated with cell cycle activation, but it is not certain how the infecting viruses interfere with cell cycling of host cells.

In brain tissues from patients with progressive multifocal leukoencephalopathy, JC virus–infected oligodendrocytes express cell cycle regulators, including Ki-67, proliferating cell nuclear antigen (PCNA), cyclin A, and cyclin B1 (24, 25). Expression of cell cycle regulators in vitro was also analyzed in studies in which JC virus was inoculated on primary human fetal astrocytes and cellular total RNA was examined by an oligonucleotide-based microarray (26). Interestingly, RNA levels of cell cycle regulators varied in a time-dependent manner during the period of virus culture. Levels of cyclin E1—the cell cycle regulator in G1/S phase—increased in the early phase of virus culture (i.e. Day 5) but decreased in the late phase (Day 15). In contrast, levels of cyclin B1—the cell cycle regulator in G2/M phase—were low on Day 5 but increased on Day 15. Thus, virus-infected cells likely proceed in the cell cycle through G1/S to G2/M phases during virus culture. Comparable temporal changes in glial cells of human brains have not been investigated in detail.

In this study, we investigated the expression of the cell cycle regulators Ki-67, PCNA, cyclin A, and cyclin B1 and of JC virus capsid proteins and oligodendrocyte lineage transcription factor 2 (OLIG2) in human brain tissues from patients with progressive multifocal leukoencephalopathy. Mildly demyelinated lesions in the brains enabled us to study early cellular changes caused by JC virus infection. The association of cell cycle regulators with progression of JC virus infection, such as nuclear size, was quantified morphometrically, and morphologic variations in PML-NBs were also examined. Accumulation of JC virus capsid proteins in PML-NBs was investigated by confocal microscopy and by recently developed fluorescence nanoscopy with ground-state depletion (GSD). Finally, progeny virion formation was observed by electron microscopy.

## MATERIALS AND METHODS

### Patients

Two autopsy cases of patients with progressive multifocal leukoencephalopathy were examined. The first case (Case 1) was a 77-year-old woman whose initial manifestations were gait abnormalities and speech disturbance. Hemiparesis developed and progressed to the point that she was unable to walk. Computed tomography examination of the brain disclosed hypodense lesions in the subcortical white matter of the left frontal lobe and the internal capsule. The lesions then extended to the right hemisphere and the brainstem. Neurologic manifestations progressed for 4 months, and she was in a vegetative state when she died. Autopsy revealed cystic lesions in the subcortical white matter of the left hemisphere and multiple degenerative lesions involving the brainstem, cerebellum, and spinal cord. JC virus was detected both by immunohistochemistry and by electron microscopy, resulting in the diagnosis of progressive multifocal leukoencephalopathy. The cause of immunosuppression associated with viral reactivation was not determined.

Case 2 was a 70-year-old woman who had mixed connective tissue disease, which included Sjögren syndrome, interstitial pneumonitis, Hashimoto thyroiditis, and systemic lupus erythematosus–like manifestations. She had been treated with corticosteroids for 3 years before the neurologic disease developed. JC virus DNA was detected from the cerebrospinal fluid by polymerase chain reaction, suggesting the diagnosis of progressive multifocal leukoencephalopathy. She died of pneumonia 6 months after the development of neurologic manifestations. At autopsy, demyelinating lesions were identified in the subcortical white matter of the bilateral hemispheres, corpus callosum, left internal capsule, cerebellum, midbrain, and pons. JC virus was detected both by immunohistochemistry and by electron microscopy.

### Autopsy of Brains

The autopsied whole brains were first fixed with 10% buffered formalin. The brain transverse sections were carefully examined macroscopically, and mildly to moderately affected areas were selected for histopathologic examination. Tissue blocks were processed and embedded in paraffin, sectioned (3–6 μm thickness), and mounted onto glass slides. The sections were then deparaffinized in xylene, rehydrated in graded alcohols, and stained with H&E, Klüver-Barrera, and Luxol fast blue/Bodian stains.

### Immunohistochemistry

For immunostaining, endogenous peroxidase activity in mounted rehydrated tissue sections was blocked with a 0.3% $H_2O_2$-methanol solution for 30 minutes at room temperature. For antigen retrieval, the sections were autoclaved in buffered citrate at 120°C for 10 minutes and incubated with primary antibodies at 4°C for approximately 12 hours. Immunohistochemistry was performed using the EnVision detection system (DakoCytomation, Glostrup, Denmark). After being thoroughly washed, the sections were incubated with a peroxidase-conjugated EnVision polymer and anti-rabbit or anti-mouse secondary antibodies (DakoCytomation) for

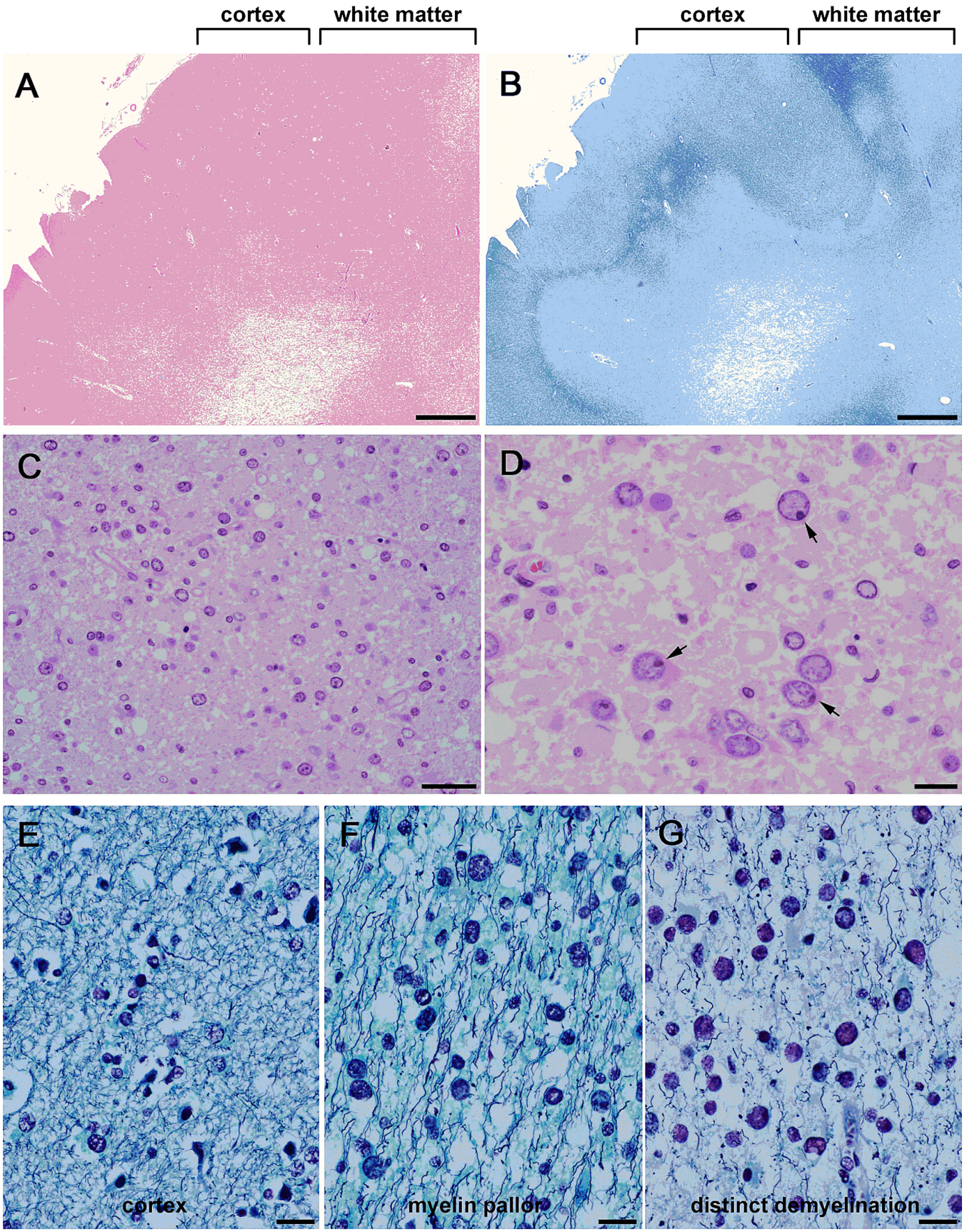

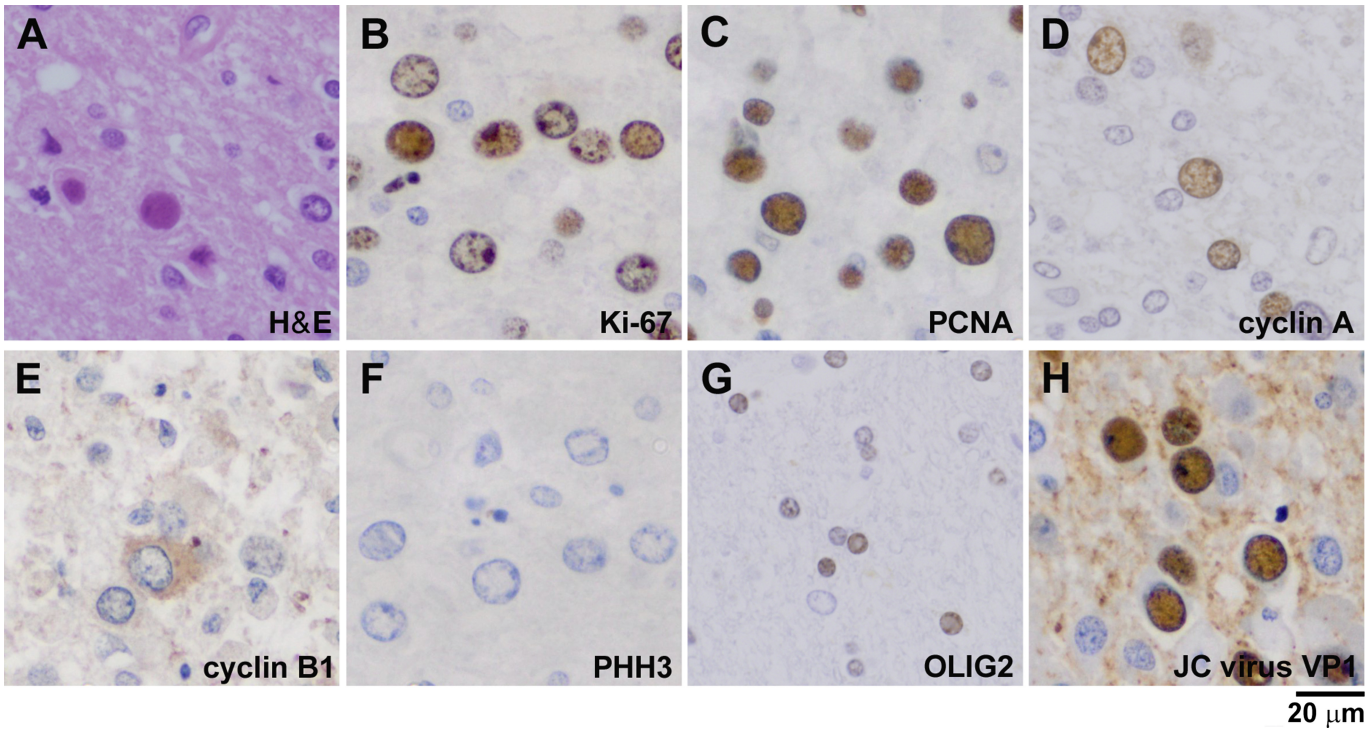


**FIGURE 2.** Expression of cell cycle regulators in nuclei of various sizes in oligodendrocytes of patients with progressive multifocal leukoencephalopathy. **(A)** Hematoxylin and eosin stain of an oligodendroglia-like cell with full viral inclusion. **(B)** Cell cycle activation, indicated by Ki-67 immunoreactivity, was detected in 22% of cells with both small and large nuclei. **(C)** Immunoreactivity to PCNA, an essential component of S phase, was detected in 68% of cells. **(D)** Immunoreactivity to cyclin A, which is involved in both S phase and G2 phase, was detected in approximately 10% of cells. **(E)** Cytoplasmic expression of cyclin B1 was detected in a few cells, but nuclear expression was not observed. **(F)** Immunoreactivity to PHH3 was not detected in the nuclei. **(G)** Immunoreactivity to OLIG2 was detected only in the small nuclei in 11% of cells. **(H)** Approximately 25% of cells were immunoreactive to the JC virus capsid protein VP1.

30 minutes at room temperature. After thorough washes, peroxidase activity was visualized with 3,3′-diaminobenzidine tetrahydrochloride (DakoCytomation).

Rabbit polyclonal antibody against the potential BC loop structure of VP1 (anti-VP1BC) has been described (21). Rabbit polyclonal antibody against VP2/VP3 was prepared against the conserved C-terminal sequence RKEGPRASSKTSYKR, as previously described (2, 22). Antibodies to the following proteins were purchased: Ki-67 (MIB-1; DakoCytomation), PCNA (Novocastra, Newcastle Upon Tyne, United Kingdom), cyclin A (Santa Cruz Biotechnology Inc, Santa Cruz, CA), cyclin B1 (Novocastra), phosphohistone H3 (PHH3; Upstate Biotechnology, Lake Placid, NY), OLIG2 (IBL, Takasaki, Japan), and PML protein (MBL, Nagoya, Japan).

## Morphometric Analysis of Immunoreactive Oligodendroglia-Like Cells

Photomicrographs of immunostained sections were taken for each protein of interest and morphometrically analyzed using MetaMorph Microscopy Automation and Image Analysis software (Molecular Devices, Sunnyvale, CA). For cells immunoreactive to JC virus VP1, OLIG2, PCNA, cyclin A, and Ki-67, images were obtained sequentially for 25 different areas using a digital camera (D1; Nikon, Tokyo, Japan) connected to a microscope with a 20× objective lens (BX-50; Olympus, Tokyo, Japan). Reactive or nonreactive signals in the micrographs were binarized and converted into black-and-white images. Only oligodendroglia-like nuclei were selected for cross-sectional nuclear area measurements using the image morphometric analysis function of the MetaMorph software. The data were transferred to a Microsoft Excel spreadsheet from which histograms were obtained.

To measure the nuclear area of cells containing punctate signals for either the PML protein or JC virus VP2/VP3, we obtained images using a digital camera (DP25; Olympus) connected to a microscope with a 40× objective lens (Axio Imager A1; Carl Zeiss, Jena, Germany). Because cells with punctate immunoreactivity could not be binarized, cross-sectional nuclear

**FIGURE 1.** Histopathology of progressive multifocal leukoencephalopathy. Low-power fields with H&E stain **(A)** and Klüver-Barrera stain **(B)** of affected brains. Mild to moderate lesions were widely distributed; there was myelin pallor in the white matter. Low magnification **(C)** and high magnification **(D)** of H&E-stained white matter show numerous oligodendroglia-like cells with enlarged nuclei. Many cells contain dot-shaped inclusions (arrows in **D**). Luxol fast blue/Bodian stain of unaffected cortex **(E)**, lesions with myelin pallor **(F)**, and lesions with distinct demyelination **(G)**. **(E)** Normal oligodendroglia have small compact nuclei. **(F)** Scattered oligodendroglia-like cells have mildly enlarged nuclei. **(G)** Many oligodendroglia-like cells have markedly enlarged nuclei. Scale bars = **(A, B)** 2 mm; **(C)** 50 μm; **(D–G)** 20 μm.

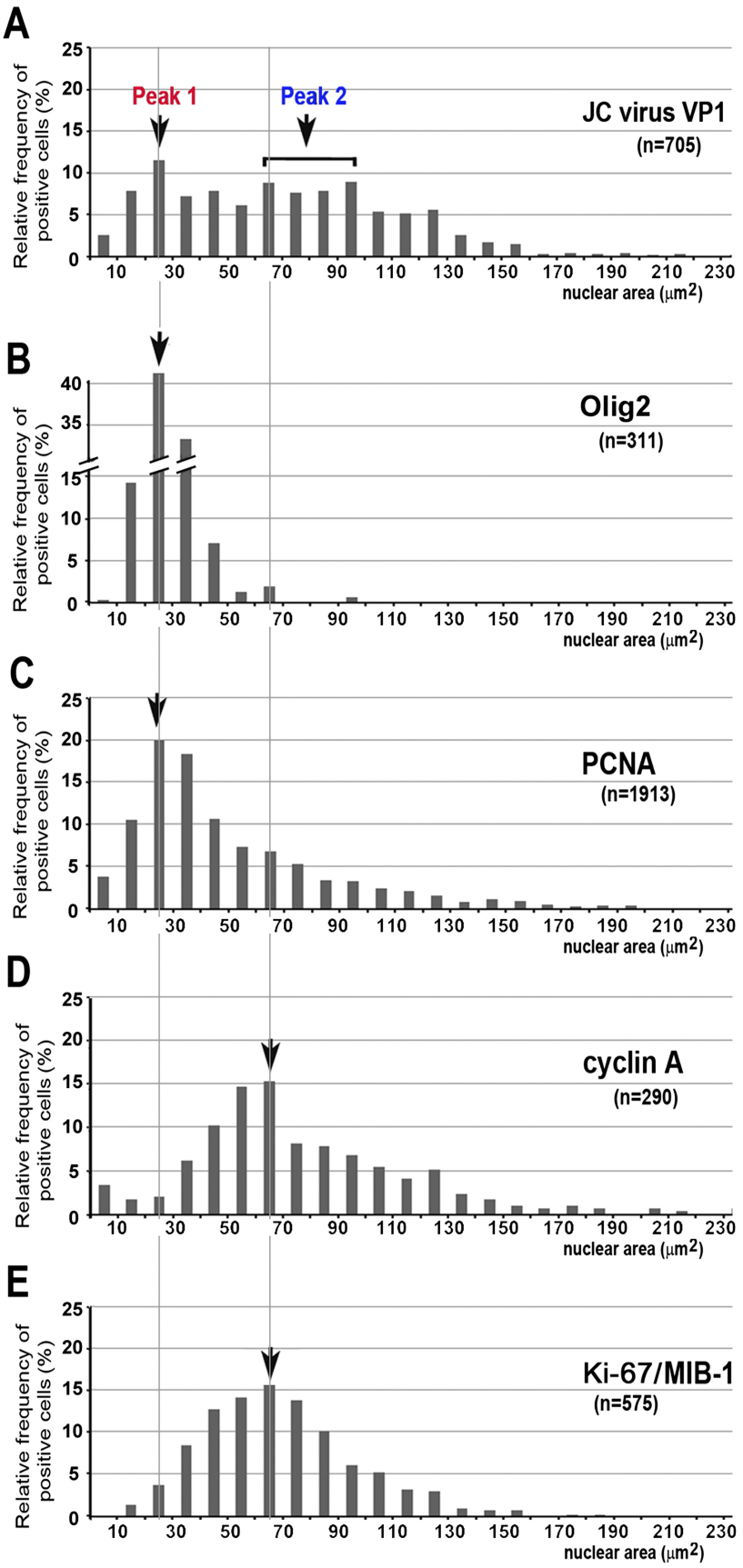

areas were measured manually for each cell by tracing the nuclear membrane. Nuclear areas were then calculated within the selected regions using the CellSens Standard DP25 controller software (Olympus).

Demyelinated lesions were more randomly scattered in the brain of Case 2, which made it difficult to collect a sufficient number of affected oligodendroglia-like cells. Thus, quantitative data were obtained mainly from Case 1; results were later confirmed in Case 2 in a limited number of cells.

### Immunofluorescence

For immunofluorescence analysis, deparaffinized and rehydrated tissue sections were blocked with PBS containing 5% normal goat serum at room temperature for 30 minutes. Then, the tissues were incubated with anti-VP2/VP3 at 4°C for approximately 12 hours, washed, and further incubated with Alexa Fluor 488–conjugated secondary antibody (Molecular Probes/Invitrogen, Carlsbad, CA). For double staining, the tissues were also incubated with anti-PML antibody followed by Alexa Fluor 568–conjugated secondary antibody (Molecular Probes/Invitrogen). After 3 washes in PBS, samples were mounted in VectaShield (Vector Laboratories, Burlingame, CA). Fluorescent images were captured using a TCS-SP confocal laser microscope (Leica, Heidelberg, Germany). The prepared slides were also analyzed using a fluorescence nanoscope with GSD in superresolution (SR GSD; Leica, Weitzlar, Germany) (27).

### Electron Microscopy

Small pieces of the formalin-fixed brain tissues were selected from mildly affected areas. The tissues were washed with PBS 3 times and then prepared for conventional electron microscopy analysis. First, the tissues were fixed with 2.5% glutaraldehyde and 1.0% paraformaldehyde in 0.1 mol/L phosphate buffer (pH 7.3) and postfixed in 1.0% osmium tetroxide. Then, the samples were dehydrated through a graded ethanol series (50%, 70%, 80%, 90%, 95%, and 100%; 3 times each) then embedded in epoxy resin. Ultrathin sections were prepared, stained with uranyl acetate and lead citrate, and examined with a JEOL 1200 EX-II electron microscope (JEOL, Tokyo, Japan).

## RESULTS

### Nuclear Enlargement of Oligodendroglia-Like Cells Is Associated With Demyelination

Postmortem brain tissue from Case 1 contained relatively mild lesions that seemed to be free from the effects of other diseases and treatment. There was mild myelin pallor in the cerebral hemispheres, and there was more distinct demyelination in the deep white matter (Figs. 1A, B). There were large numbers of oligodendroglia-like cells with variable nuclear sizes in the white matter lesions. Most of these cells showed clear nucleoplasm with chromatin marginated to the rims of the nuclear membranes (Figs. 1C, D). Many of these nuclei also appeared to contain dot-shaped viral inclusions that were frequently observed at the inner peripheral areas of the nuclei close to the nuclear membranes (Fig. 1D). The proportion of nuclei containing full viral inclusions was markedly small, as determined by H&E staining (Fig. 2A), but more glial cells were confirmed to be immunoreactive to the JC virus capsid proteins VP1 and VP2/VP3 (Figs. 2, 5).

We next compared the nuclear sizes of oligodendroglia-like cells and degrees of demyelination in sections stained with Luxol fast blue/Bodian. In the unaffected cerebral cortex, oligodendroglia showed normal-sized nuclei with rare nuclear enlargement (Fig. 1E). In the white matter with myelin pallor, oligodendroglia-like cells had more variable nuclear sizes (Fig. 1F). In the deep white matter with distinct demyelination, even more oligodendroglia-like cells had marked nuclear enlargement (Fig. 1G). Thus, nuclear enlargement was likely associated with advancement of demyelination. Similar cytopathologic alterations were found in tissues from Case 2, although demyelinated lesions were more randomly scattered in the white matter.

### Expression of Cell Cycle Regulators in Nuclei of Various Sizes

Expression of cell cycle regulators was next examined with immunohistochemistry. Oligodendroglia-like cells were first investigated for immunoreactivity to glial fibrillary acidic protein (GFAP) and were found to be GFAP–negative (data not shown). The cells displayed round or oval-shaped nuclei, which are characteristic of oligodendrocytes (Fig. 2A). There were a small number of GFAP–positive astroglia, which showed JC virus inclusions in their enlarged nuclei (data not shown). The nuclei of infected astroglia, however, were more irregularly shaped and much larger than oligodendroglia-like cells. Thus, in the next analysis, only cells with oligodendroglia-like round or oval nuclei were selected, and those of distinct astroglia or other cells (such as macrophages) were excluded.

The cell cycle stages were examined by assessing the expression of the cell cycle regulators Ki-67, PCNA, cyclin A, cyclin B1, and PHH3. Ki-67 expression indicates cell cycle activation besides the resting state G0. Among 2,808 cells with oligodendroglia-like nuclei, Ki-67 immunoreactivity was detected in 605 cells (22%), but it was absent in normal oligodendroglia with small nuclei (Fig. 2B). Proliferating cell nuclear antigen (PCNA), an essential component of DNA replication during S phase, was detected in the nuclei of 1,913 (68%) of 2,810 cells (Fig. 2C). Cyclin A, which is involved in both S phase and G2 phase, must be degraded upon entry into mitosis (28, 29). Cyclin A was detected in the nuclei of 290 (10%) of 2,800 cells (Fig. 2D). To identify the cells entering mitosis, we also examined immunoreactivity to cyclin B1 and PHH3. Cyclin B1 initially localizes to the cytoplasm but

**FIGURE 3.** Cell cycle transition through an S-to-G2–like state with nuclear enlargement. Distribution of cells immunoreactive to JC virus VP1 **(A)**, OLIG2 **(B)**, PCNA **(C)**, cyclin A **(D)**, and Ki-67 **(E)**, in relation to cross-sectional nuclear area. In cells immunoreactive to JC virus VP1, 2 populations were operationally designated as Peak 1 (20–30 $\mu m^2$) and Peak 2 (60–100 $\mu m^2$). Cells immunoreactive to OLIG2 **(B)** and PCNA **(C)** showed the highest relative frequency in nuclei ranging from 20 to 30 $\mu m^2$. In contrast, cells immunoreactive to cyclin A **(D)** and Ki-67 **(E)** showed the highest relative frequency in nuclei ranging from 60 to 70 $\mu m^2$.

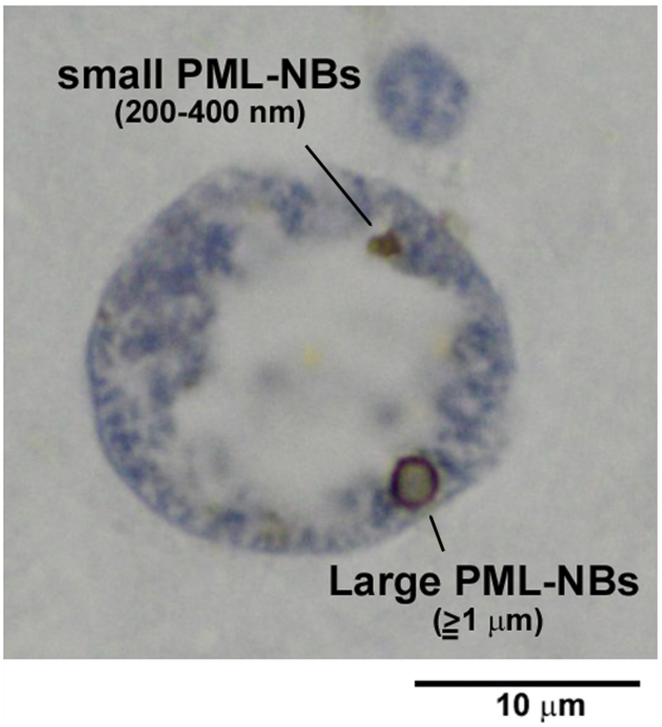


**FIGURE 4.** Small and large PML-NBs in an enlarged oligodendroglial nucleus. Immunohistochemistry for the PML protein demonstrates 2 types of PML-NBs: small (~200–300 nm in diameter) and large (≥1 μm in diameter). Ringlike structures with pale central cores are apparent in 2-dimensional sections (100× objective lens with oil immersion).

accumulates in the nucleus in late G2 phase, which is a prerequisite for mitotic initiation in mammalian cells (30). In oligodendroglia-like cells, cyclin B1 was observed only in the cytoplasm and/or in the perinuclear rim of a small number of enlarged nuclei, and nuclear expression was not detected (Fig. 2E). Nuclear immunoreactivity of PHH3, a marker of the mitotic state, was also not detected (Fig. 2F).

To further characterize oligodendroglia-like cells, we examined the expression of OLIG2. Oligodendrocyte lineage transcription factor 2 (OLIG2) is a basic helix-loop-helix transcription factor that regulates the differentiation of oligodendroglia with enhanced myelin production (31, 32). Among the 2,810 cells examined, OLIG2 immunoreactivity was detected in 311 mostly normal-appearing oligodendroglia with small nuclei (11%) but was not detected in those with enlarged nuclei (Fig. 2G). The JC virus major capsid protein VP1 was detected in 704 (25%) of 2,808 cells (Fig. 2H). Importantly, VP1 immunoreactivity was detected in cells with smaller nuclei and in those with markedly enlarged nuclei.

## Cell Cycle Transition Through an S-to-G2–Like State With Nuclear Enlargement

Because nuclear enlargement of oligodendroglia seemed to be associated with advancement of demyelination (Figs. 1E–G), we examined the relationships between nuclear size and expression of JC virus VP1 or cell cycle regulators. Nuclear size was estimated from cross-sectional nuclear areas of each immunoreactive cell; the results are presented as histograms with cross-sectional areas in the abscissa and its relative frequency in the ordinate (Fig. 3).

JC virus VP1 immunoreactivity was detected in cells with a wide range of nuclear sizes, but quantification of nuclear areas indicated that there were roughly 2 populations, which we operationally designated as Peak 1 and Peak 2. Peak 1 contained cells with nuclei ranging from 20 to 30 $\mu m^2$, and Peak 2 contained cells with nuclei ranging from 60 to 100 $\mu m^2$ (Fig. 3A).

The cells in Peak 1 tended to be immunoreactive to OLIG2 and PCNA. Expression of OLIG2 was almost entirely restricted to cells with small nuclei, with more than 40% of OLIG2-immunoreactive cells having nuclei ranging from 20 to 30 $\mu m^2$ (Fig. 3B). In contrast, the cells immunoreactive to PCNA showed more variable nuclear sizes. Although 20% of PCNA-immunoreactive cells were included in Peak 1, PCNA was also detected in cells with nuclei as large as 200 $\mu m^2$ (Fig. 3C).

The cells in Peak 2, in contrast, were more closely related to the expression of cyclin A and Ki-67. For both cyclin A and Ki-67, approximately 15% of immunoreactive cells had nuclei ranging from 60 to 70 $\mu m^2$; however, in both cases, immunoreactivity was also detected in cells with nuclei larger than 150 $\mu m^2$ (Figs. 3D, E).

Taken together, the results presented in Figures 2 and 3 indicate that the cell cycle likely proceeds in association with nuclear enlargement. Soon after initiation of nuclear enlargement, oligodendroglia may diminish myelin production activities by reducing OLIG2 expression and may instead proceed through the cell cycle through an S-to-G2-like state with expression of PCNA and cyclin A, respectively. Entry into late G2 state and M state was not apparent based on the absence of the nuclear expression of cyclin B1 and PHH3. The presence of 2 nuclear size peaks in the expression of the JC virus capsid protein VP1 may indicate 2 regulatory phases for viral progeny production relating to S state and G2-like state.

## Small and Large PML-NBs in Enlarging Nuclei of Oligodendrocytes

In oligodendroglia-like cells of JC virus–infected human brain tissues, PML-NBs were detected as punctate structures of various sizes but frequently appeared as 1 of 2 types of immunoreactivity to the PML protein, an essential component of PML-NBs. There were granular regions 200 to 400 nm in diameter (small PML-NBs) or large circular structures with diameters of 1 μm or more (large PML-NBs). Both types of PML-NBs exhibited ring-shaped structures in 2-dimensional sections, with a pale central core that was more apparent in large PML-NBs (Fig. 4).

We next examined the possible relationships of morphologic variations in PML-NBs with nuclear sizes. Coexistence of small and large PML-NBs was observed in cells with a wide range of nuclear sizes (Figs. 4, 5B–D), but small PML-NBs were more frequently observed in the smaller nuclei and large PML-NBs were more frequently observed in the larger nuclei. Nuclei smaller than 50 $\mu m^2$ contained only small PML-NBs (Fig. 5A), whereas nuclei larger than 200 $\mu m^2$ contained only large PML-NBs (Fig. 5E). For quantification,

the sizes of PML-NBs were categorized into diameters less than 1 μm and diameters of 1 μm or more, and nuclear areas containing PML-NBs were measured. The mean ± SD nuclear area of nuclei containing PML-NBs less than 1 μm in diameter was 51.0 ± 30.4 $\mu m^2$ (n = 43); most PML-NBs were as small as 200 to 400 nm in diameter (small PML-NBs). In contrast, the mean ± SD nuclear area of nuclei containing PML-NBs with diameters of 1 μm or more (large PML-NBs) was 136.7 ± 75.8 $\mu m^2$ (n = 21). Nuclei containing PML-NBs both less than 1 μm (small PML-NBs) and 1 μm or more (large PML-NBs) were measured twice for each group.

Intranuclear viral inclusions also showed morphologic variability, which we examined in relation to nuclear size. Viral inclusions were visualized with an antibody that recognizes the common C-terminal sequence of the minor capsid proteins VP2 and VP3. This antibody allowed better discrimination of inclusions than the VP1 antibody (2, 22). In nuclei usually smaller than 50 $\mu m^2$, only faint diffuse VP2/VP3 immunoreactivity was observed (Fig. 5F). In nuclei approximately 50 to 90 $\mu m^2$, there were granular VP2/VP3 signals resembling small PML-NBs (Figs. 5G, H). Distinct dot-shaped inclusions (≥1 μm in diameter) appeared in nuclei larger than 60 $\mu m^2$; their VP2/VP3 signals resembled those of large PML-NBs (Figs. 5G, H). In the obviously enlarged nuclei larger than 100 $\mu m^2$, the viral capsid proteins were detected throughout the nuclei, with occasional nuclei containing large fused dot-shaped signals (Figs. 5I, J). The mean ± SD nuclear area of the 34 oligodendroglia-like cells with clear JC virus dot-shaped inclusions (>1 μm in diameter) was 91.8 ± 25.5 $\mu m^2$ (Fig. 5K). Importantly, this size range corresponded to Peak 2

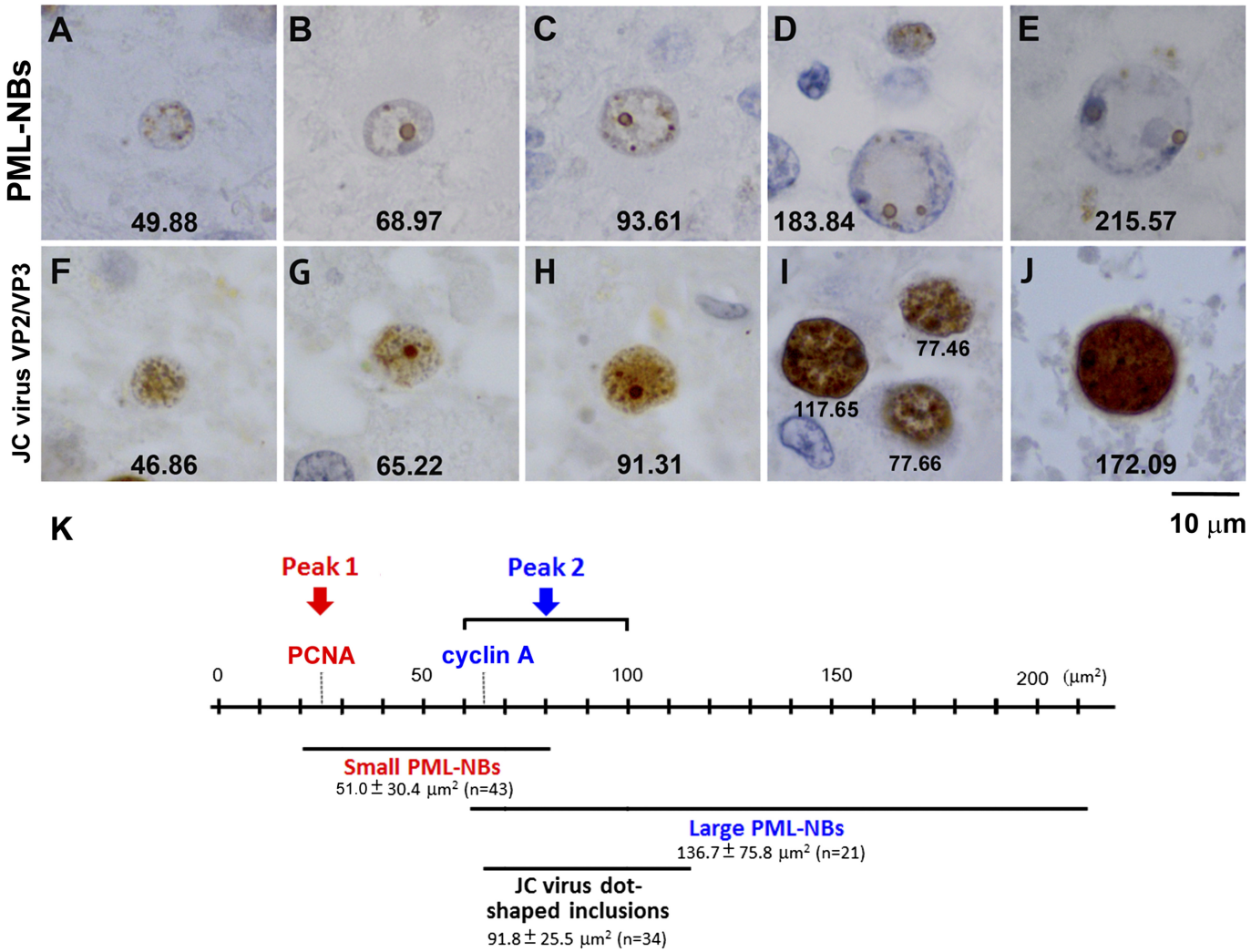


**FIGURE 5.** Morphologic variations in PML-NBs and JC virus nuclear inclusions. **(A–E)** Immunohistochemistry for the PML protein. Coexistence of small and large PML-NBs is frequently observed in cells with a wide range of nuclear sizes; large PML-NBs are more frequently observed in larger nuclei and small PML-NBs are more numerous in smaller nuclei. The numbers in each panel indicate the cross-sectional areas (in square micrometers) of the individual nuclei. **(F–J)** Immunohistochemistry for the JC virus capsid proteins VP2/VP3. JC virus capsid protein is detected in small nuclei **(F)**, but signal intensity is relatively weak. Dot-shaped viral inclusions are present in the nuclei in **(G)** to **(J)**. As nuclear areas increase, there is more diffuse JC virus capsid protein signal intensity, making the dot-shaped signals less apparent. **(K)** Schematic representation of the observed relationships among nuclear area, PCNA and cyclin A expression, PML-NB size, and dot-shaped JC virus nuclear inclusions.

in Figure 3 (60–100 $\mu m^2$) and also to the nuclear size range in which large PML-NBs begin to appear (136.7 ± 75.8 $\mu m^2$).

## JC Virus Disrupts Scaffolding of Large PML-NBs During Full Inclusion Formation

We next analyzed the relationship between the development of intranuclear viral inclusions and PML-NBs (Fig. 6). Brain tissues double-stained for JC virus VP2/VP3 and PML protein were analyzed by confocal microscopy. Consistent with the data presented in Figure 4, the PML protein was detected as both small and large ringlike structures in 2-dimensional sections and as spherical shells in 3 dimensions. In smaller nuclei, small PML-NBs that colocalized with faint capsid protein signals were observed (Fig. 6A, arrow 1). In larger nuclei, large PML-NBs developed preferentially at the inner nuclear periphery; dot-shaped viral inclusions were clearly detected in association with large PML-NBs (Fig. 6B, arrow 2). There were also cells that contained full viral inclusions in the enlarged nuclei. In these cells, strong signals for JC virus capsid proteins were diffusely detected throughout the nucleus, but immunoreactivity to the PML protein was too weak to be visualized (3 cells indicated by arrow 3 in Figs. 6A, B).

The viral inclusions were examined in more detail with the use of a fluorescence nanoscope with GSD (27) (Fig. 7). In 1 nucleus, 2 dot-shaped viral inclusions were observed (arrows 1 and 2 in Fig. 7). Both were associated with large ringlike immunoreactivity to the PML protein, but the PML-NBs appeared to be in different stages. In one, a distinct ringlike structure, approximately 2 μm in diameter, was apparent (arrow 1); in the other, a faint ringlike structure was focally disrupted, and PML protein immunoreactivity seemed to be disappearing (arrow 2). Thus, the data presented in Figures 6 and 7 indicate that PML-NBs provide a scaffold for JC virus progeny production and that these structures are disrupted in the process of full viral inclusion formation.

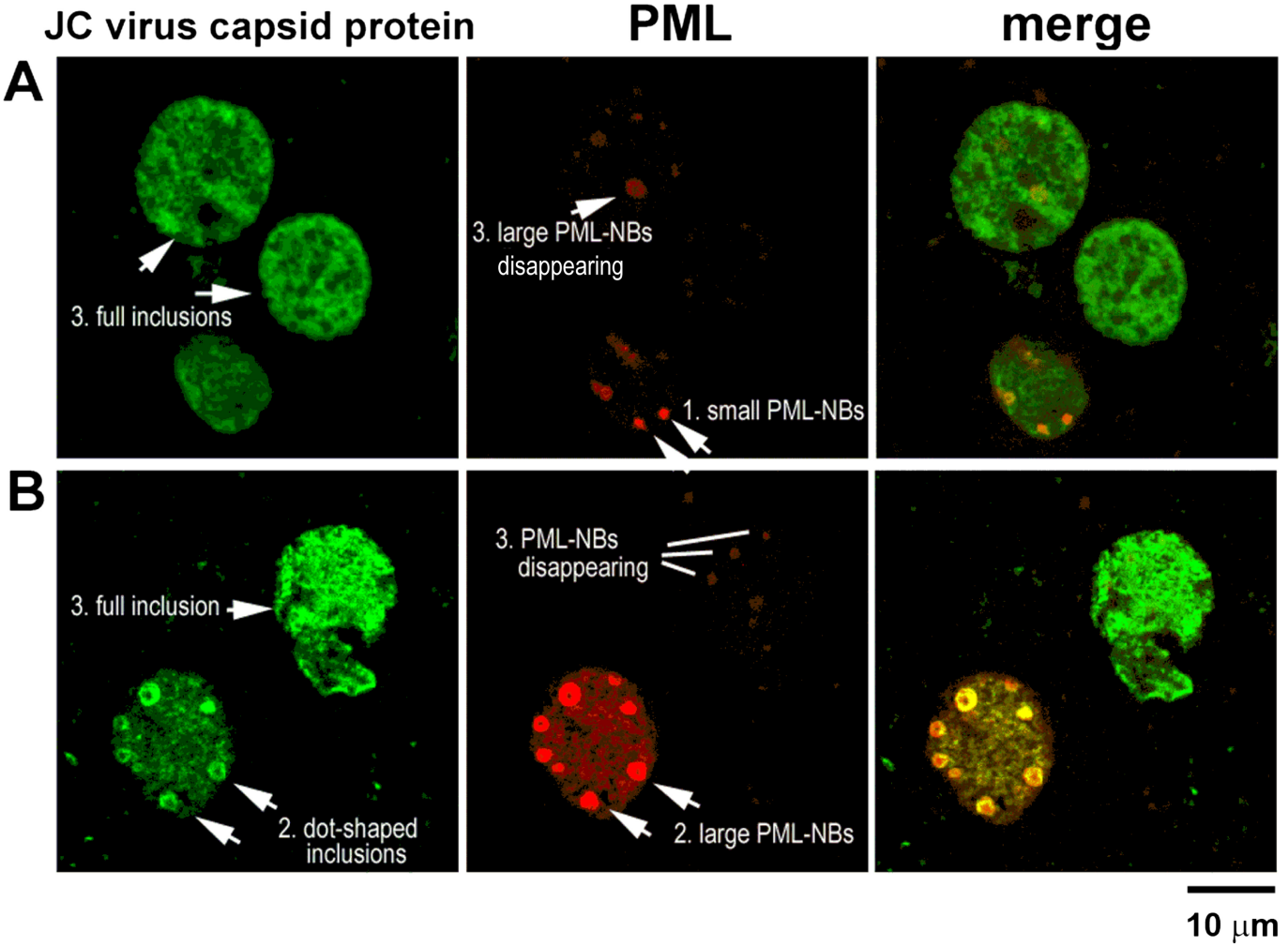


**FIGURE 6.** Association of viral inclusions with PML-NBs. **(A, B)** Distribution of the JC virus capsid proteins VP2/VP3 (green) and the PML protein (red) in nuclei. In smaller nuclei, granular PML-NB–like structures are weakly immunoreactive to JC virus capsid proteins (**A**, arrow 1). As nuclei enlarge, dot-shaped viral inclusions are detected in association with large PML-NBs (**B**, arrow 2). In large nuclei with full viral inclusions, PML-NBs are disrupted or disappear (**A, B,** 3 cells with arrow 3).

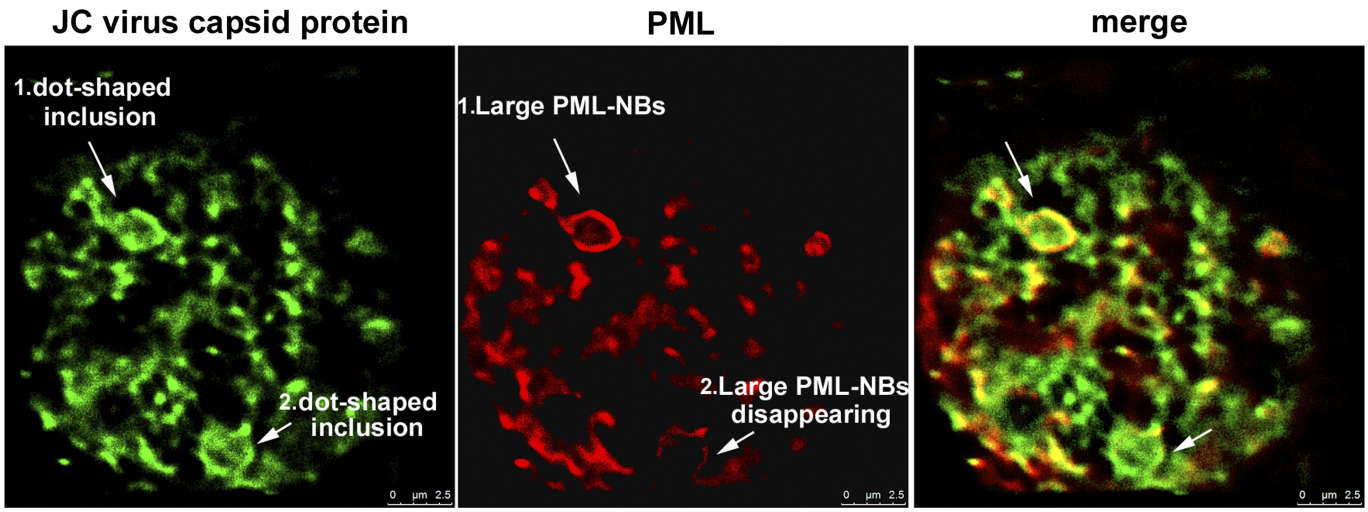


**FIGURE 7.** Disruption of PML-NBs in the process of full inclusion formation. Distributions of the JC virus capsid proteins VP2/VP3 (green) and the PML protein (red) were analyzed with a superresolution GSD nanoscope. Two large PML-NBs associated with dot-shaped viral inclusions were observed in enlarged nuclei: one displayed a distinct ringlike structure more than 2 μm in diameter (arrow 1), whereas the other showed a disrupting PML-NB structure with decreased intensity of the PML protein (arrow 2).

### JC Virus Progenies Form Clusters of Various Sizes in the Nuclei

The brain tissues from Cases 1 and 2 were examined by electron microscopy. In both cases, progeny virions were observed to form electron-dense clusters ranging from approximately 200 nm to more than 1 μm in diameter, corresponding to the size of small and large PML-NBs detected by confocal microscopy and GSD fluorescence nanoscopy (Figs. 8A, B). The larger clusters tended to be observed at the inner periphery of the nucleus. Clustered progeny virions with round structures were apparent at high magnification (Fig. 8C). These results consistently indicate that viral progeny production initiates in small PML-NBs and continues as PML-NBs grow into large spherical shells.

## DISCUSSION

We have demonstrated that JC virus produces progeny virions in association with PML-NBs. Intranuclear viral inclusions likely develop with cell cycle progression through an S-to-G2–like state, whereas PML-NBs grow larger in enlarging nuclei. These gradual changes have been difficult to investigate in most autopsy cases because oligodendrocytes have already developed full viral inclusions in areas of distinct demyelination or because infected cells are severely damaged in burnt-out lesions. Fortunately, however, in the autopsy cases of the present study, pathologic analysis of the brains demonstrated relatively mild demyelinated lesions. A large number of glial cells with dot-shaped JC virus inclusions were detected, and the early stages of viral inclusion formation could be analyzed (Fig. 1).

Our results indicate that, in oligodendroglia in the brains of patients with progressive multifocal leukoencephalopathy, the cell cycle is activated and proceeds through an S-to-G2–like state in association with nuclear enlargement (Figs. 2, 3). Although temporal changes could not be directly observed in these formalin-fixed tissues, our results are consistent with previous in vitro findings suggesting that DNA viruses activate the cell cycle of resting host cells and promote entry into S phase early during infection. For example, simian virus 40 large T antigen promoted entry into S phase (33), and cells infected with mouse polyomavirus or simian virus 40 accumulated in S and G2/M phases (34). More recently, JC virus was shown to proliferate progeny in G2-arrested host cells (35). The present study consistently demonstrates virus infection–associated cell cycle modulation in human brain tissues and is the first to show an association between virus-induced cell cycle changes and nuclear enlargement.

Importantly, this study also describes morphologic variations in PML-NBs in relation to nuclear size. Sizes of PML-NBs are variable, but they were frequently detected as small (200–400 nm in diameter) or large (>1 μm) spherical shells (Fig. 4). Large PML-NBs more than 1 μm in diameter were detected in vitro in BK virus–infected rat primary kidney tubule epithelial cells (36) and in polyomavirus-infected cells (37). JC virus–infected oligodendroglia-like cells also consistently showed markedly enlarged PML-NBs in the human brain tissues that seemed to grow in association with the cell cycle transition through an S-to-G2–like state (Fig. 5). Markedly enlarged, spherically shaped PML-NBs also appear in G2 phase in lymphocytes of patients with immunodeficiency, centromeric instability, and facial anomalies syndrome, and large PML-NBs were found to be organized, with protein layers surrounding a core of satellite DNA (38). Enlargement of PML-NBs is likely an anti-stress response, but it is unclear why the cells in the brains of patients with progressive multifocal leukoencephalopathy undergo cell death rather than proceeding to mitosis.

JC virus capsid proteins and virion clusters were associated with PML-NBs of different sizes (Figs. 5–7), suggesting a continuous scaffolding role for PML-NBs in JC virus progeny production. Promyelocytic leukemia nuclear bodies are known to perform multiple roles that vary when cells are infected with different viruses. For example, in neuronal cells

 

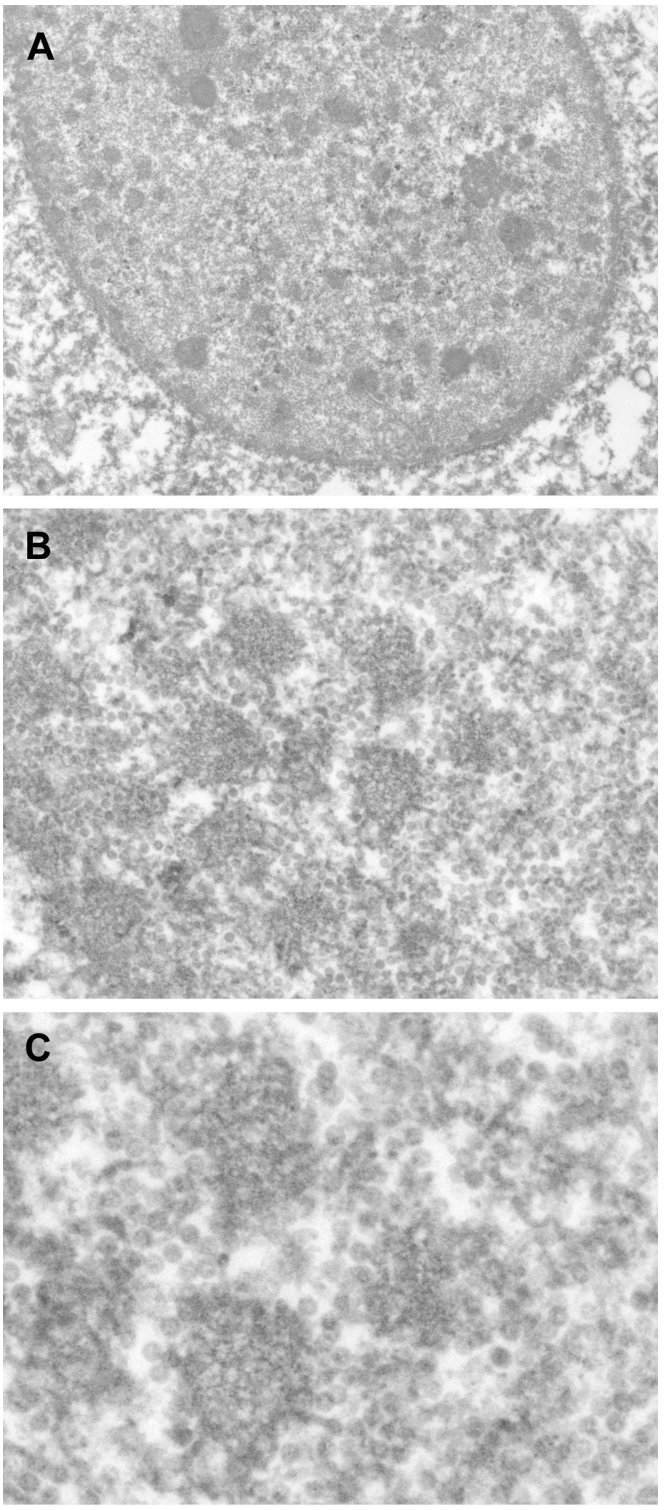


**FIGURE 8.** Clusters of JC virus progeny virions observed by electron microscopy. JC virus progeny virions were detected as clusters ranging from approximately 200 nm to more than 1 μm. The size of viral clusters correlated with the size of PML-NBs, suggesting that viral progeny production occurs in association with growing PML-NBs. Scale bars = **(A)** 1 μm; **(B)** 250 nm; **(C)** 50 nm.

infected with herpes viruses, such as herpes simplex virus type 1 and varicella zoster virus, the viral genomic DNA or the nucleocapsids were detected inside large PML-NBs, suggesting that PML-NBs are involved in herpes simplex virus type 1 viral latency control (39) or serve as an intrinsic antiviral host defense response against varicella zoster virus infection (40). In contrast, JC virus lytic infection indicated structural roles for PML-NBs in providing scaffolding for viral progeny production, but depletion of the *pml* gene from host cells in in vitro experiments did not dramatically affect the replication of JC virus, BK virus, or polyomavirus; therefore, PML-NBs would not be essential for viral replication (36, 37, 41). If that is the case, a question arises: ''What is the role of PML-NBs in JC virus infection?'' Although it is unclear whether PML-NBs play proviral or antiviral roles, we think that PML-NBs are related more to antiviral defense and subsequent cell death mechanisms than to scaffolding for viral progeny production.

In JC virus–infected oligodendroglia-like cells, PML-NB structures appeared to be disrupted once sufficient viral progeny had been produced (Figs. 6–8). Disruption of PML-NBs is partly related to the function of a small viral regulatory protein called ''agnoprotein.'' Our previous experiments in vitro indicated that the agnoprotein enhances efficient progeny production in PML-NBs and subsequent cell death. With depletion of the agnogene, ectopic capsid assembly outside the PML-NBs occurred, and host cell degradation seemed to be minimized (4). Other investigators reported similar data in which the agnoprotein-depleted mutant released virions that were mostly deficient in viral genomic DNA (42) or the agnoprotein induced dysregulated cell cycling of the host cells (43). Because PML-NBs are involved in multiple nuclear events, including cell cycle progression, chromatin regulation, transcription, DNA replication and repair, tumor suppression, apoptosis, and telomere lengthening (8), virus-induced PML-NB disruption would cause fatal damage to host cells. However, the damage to host cells would be initiated much earlier than the recognized structural disruption of PML-NBs, as observed in BK virus–infected cells, in which PML-NBs are reorganized in association with active viral DNA replication (37). Abundant viral DNA synthesis may influence host cell genome duplication in S phase and can induce cell cycle dysregulation. Thus, arrest of entry into M phase would be determined much earlier than PML-NB disruption; however, the mechanism of virus-induced cell death is still unclear.

In summary, we present data indicating that early changes in JC virus–infected oligodendroglia are associated with cell cycle progression through an S-to-G2–like state. In enlarging nuclei, PML-NBs (where JC virus produces progeny virions) also enlarge. The PML-NB structures eventually dissociate with full viral inclusion formation. These findings may help us understand the pathologic mechanisms of virus-induced cell death and may also contribute to the early diagnosis of progressive multifocal leukoencephalopathy.

## ACKNOWLEDGMENTS

*We thank Sayuri Koroishi and Yukie Matsubara (Laboratory of Electron Microscopy, Kyorin University, Tokyo, Japan) for technical assistance with electron microscopy.*

## REFERENCES


1. Ferenczy MW, Marshall LJ, Nelson CD, et al. Molecular biology, epidemiology, and pathogenesis of progressive multifocal leukoencephalopathy, the JC virus–induced demyelinating disease of the human brain. Clin Microbiol Rev 2012;25:471–506
2. Shishido-Hara Y, Higuchi K, Ohara S, et al. Promyelocytic leukemia nuclear bodies provide a scaffold for human polyomavirus JC replication and are disrupted after development of viral inclusions in progressive multifocal leukoencephalopathy. J Neuropathol Exp Neurol 2008;67:299–308
3. Shishido-Hara Y. Progressive multifocal leukoencephalopathy and promyelocytic leukemia nuclear bodies: A review of clinical, neuropathological, and virological aspects of JC virus–induced demyelinating disease. Acta Neuropathol 2010;120:403–17
4. Shishido-Hara Y, Ichinose S, Uchihara T. JC virus intranuclear inclusions associated with PML-NBs: Analysis by electron microscopy and structured illumination microscopy. Am J Pathol 2012;180:1095–106
5. Novoa RR, Calderita G, Arranz R, et al. Virus factories: Associations of cell organelles for viral replication and morphogenesis. Biol Cell 2005;97:147–72
6. de Castro IF, Volonte L, Risco C. Virus factories: Biogenesis and structural design. Cell Microbiol 2013;15:24–34
7. Lallemand-Breitenbach V, de The H. PML nuclear bodies. Cold Spring Harb Perspect Biol 2010;2:a000661
8. Van Damme E, Laukens K, Dang TH, et al. A manually curated network of the PML nuclear body interactome reveals an important role for PML-NBs in SUMOylation dynamics. Int J Biol Sci 2010;6:51–67
9. Reineke EL, Kao HY. Targeting promyelocytic leukemia protein: A means to regulating PML nuclear bodies. Int J Biol Sci 2009;5:366–76
10. Bernardi R, Papa A, Pandolfi PP. Regulation of apoptosis by PML and the PML-NBs. Oncogene 2008;27:6299–312
11. Bernardi R, Pandolfi PP. Structure, dynamics and functions of promyelocytic leukaemia nuclear bodies. Nat Rev Mol Cell Biol 2007;8:1006–16
12. Dellaire G, Ching RW, Dehghani H, et al. The number of PML nuclear bodies increases in early S phase by a fission mechanism. J Cell Sci 2006;119:1026–33
13. Lang M, Jegou T, Chung I, et al. Three-dimensional organization of promyelocytic leukemia nuclear bodies. J Cell Sci 2010;123:392–400
14. Dellaire G, Eskiw CH, Dehghani H, et al. Mitotic accumulations of PML protein contribute to the re-establishment of PML nuclear bodies in G1. J Cell Sci 2006;119:1034–42
15. Chen YC, Kappel C, Beaudouin J, et al. Live cell dynamics of promyelocytic leukemia nuclear bodies upon entry into and exit from mitosis. Mol Biol Cell 2008;19:3147–62
16. Wang S, Long J, Zheng CF. The potential link between PML NBs and ICP0 in regulating lytic and latent infection of HSV-1. Protein Cell 2012;3:372–82
17. Frappier L. Viral disruption of promyelocytic leukemia (PML) nuclear bodies by hijacking host PML regulators. Virulence 2011;2:58–62
18. Tavalai N, Stamminger T. Interplay between herpesvirus infection and host defense by PML nuclear bodies. Viruses 2009;1:1240–64
19. Everett RD, Chelbi-Alix MK. PML and PML nuclear bodies: Implications in antiviral defence. Biochimie 2007;89:819–30
20. Shishido Y, Nukuzuma S, Mukaigawa J, et al. Assembly of JC virus–like particles in COS7 cells. J Med Virol 1997;51:265–72
21. Shishido-Hara Y, Hara Y, Larson T, et al. Analysis of capsid formation of human polyomavirus JC (Tokyo-1 strain) by a eukaryotic expression system: Splicing of late RNAs, translation and nuclear transport of major capsid protein VP1, and capsid assembly. J Virol 2000;74:1840–53
22. Shishido-Hara Y, Ichinose S, Higuchi K, et al. Major and minor capsid proteins of human polyomavirus JC cooperatively accumulate to nuclear domain 10 for assembly into virions. J Virol 2004;78:9890–903
23. Jul-Larsen A, Visted T, Karlsen BO, et al. PML-nuclear bodies accumulate DNA in response to polyomavirus BK and simian virus 40 replication. Exp Cell Res 2004;298:58–73
24. Ariza A, Mate JL, Fernandez-Vasalo A, et al. p53 and proliferating cell nuclear antigen expression in JC virus–infected cells of progressive multifocal leukoencephalopathy. Hum Pathol 1994;25:1341–45
25. Ariza A, Mate JL, Isamat M, et al. Overexpression of Ki-67 and cyclins A and B1 in JC virus–infected cells of progressive multifocal leukoencephalopathy. J Neuropathol Exp Neurol 1998;57:226–30
26. Radhakrishnan S, Otte J, Enam S, et al. JC virus–induced changes in cellular gene expression in primary human astrocytes. J Virol 2003;77:10638–44
27. Folling J, Bossi M, Bock H, et al. Fluorescence nanoscopy by ground-state depletion and single-molecule return. Nat Methods 2008;5:943–45
28. Mateo F, Vidal-Laliena M, Pujol MJ, et al. Acetylation of cyclin A: A new cell cycle regulatory mechanism. Biochem Soc Trans 2010;38:83–86
29. Pagano M, Pepperkok R, Verde F, et al. Cyclin A is required at two points in the human cell cycle. EMBO J 1992;11:961–71
30. Taylor WR, Stark GR. Regulation of the G2/M transition by p53. Oncogene 2001;20:1803–15
31. Wegner M. Expression of transcription factors during oligodendroglial development. Microsc Res Tech 2001;52:746–52
32. Wegner M. A matter of identity: Transcriptional control in oligodendrocytes. J Mol Neurosci 2008;35:3–12
33. Dickmanns A, Zeitvogel A, Simmersbach F, et al. The kinetics of simian virus 40–induced progression of quiescent cells into S phase depend on four independent functions of large T antigen. J Virol 1994;68:5496–508
34. Lehman JM, Laffin J, Friedrich TD. DNA content distribution of mouse cells following infection with polyoma virus. Cytometry 1994;16:138–43
35. Orba Y, Suzuki T, Makino Y, et al. Large T antigen promotes JC virus replication in G2-arrested cells by inducing ATM- and ATR-mediated G2 checkpoint signaling. J Biol Chem 2010;285:1544–54
36. Jiang M, Entezami P, Gamez M, et al. Functional reorganization of promyelocytic leukemia nuclear bodies during BK virus infection. MBio 2011;2:e00281–10
37. Erickson KD, Bouchet-Marquis C, Heiser K, et al. Virion assembly factories in the nucleus of polyomavirus-infected cells. PLoS Pathog 2012;8:e1002630
38. Luciani JJ, Depetris D, Usson Y, et al. PML nuclear bodies are highly organised DNA-protein structures with a function in heterochromatin remodelling at the G2 phase. J Cell Sci 2006;119:2518–31
39. Catez F, Picard C, Held K, et al. HSV-1 genome subnuclear positioning and associations with host-cell PML-NBs and centromeres regulate LAT locus transcription during latency in neurons. PLoS Pathog 2012;8:e1002852
40. Reichelt M, Wang L, Sommer M, et al. Entrapment of viral capsids in nuclear PML cages is an intrinsic antiviral host defense against varicella-zoster virus. PLoS Pathog 2011;7:e1001266
41. Gasparovic ML, Maginnis MS, O'Hara BA, et al. Modulation of PML protein expression regulates JCV infection. Virology 2009;390:279–88
42. Sariyer IK, Saribas AS, White MK, et al. Infection by agnoprotein-negative mutants of polyomavirus JC and SV40 results in the release of virions that are mostly deficient in DNA content. Virol J 2011;8:255
43. Darbinyan A, Darbinian N, Safak M, et al. Evidence for dysregulation of cell cycle by human polyomavirus, JCV, late auxiliary protein. Oncogene 2002;21:5574–81


 